ACS Photonics

Article

pubs.acs.org/journal/apchd5

Two-Photon Luminescence of Gold Nanorods Mediated by Higher Order Plasmon Modes

Niels Verellen,*[,‡,†] Denitza Denkova,[†] Ben De Clercq,[§] Alejandro V. Silhanek,[∥] Marcel Ameloot,[§] Pol Van Dorpe,[‡,†] and Victor V. Moshchalkov[†]

[†]INPAC and Dept. of Physics, KU Leuven, Celestijnenlaan 200 D, B-3001 Leuven, Belgium

[‡]IMEC, Kapeldreef 75, B-3001 Leuven, Belgium

[§]University Hasselt and Transnational University Limburg, BIOMED, Diepenbeek, Belgium

[∥]Département de Physique, Université de Liège, Sart Tilman, B-4000 Liège, Belgium

ABSTRACT: Metallic nanorod antennas can be considered as an analogue to classical half-wave dipole antennas, constituting an important tool for manipulating linear and nonlinear light-matter interactions in nanoscale volumes. Using two-photon luminescence (TPL) scanning laser microscopy, we investigate such optical antennas beyond their fundamental dipole mode. The antenna mode dispersion is extracted from the nonlinear TPL measurement and reveals a TPL process that is dominated by plasmon-induced enhancement of the two-photon absorption in the metal. Additionally, a clear signature of the mode parity is observed in the TPL images. TPL maxima are observed outside the antenna boundaries for even parity modes, whereas they are located inside for odd modes. It is concluded that for even modes the two-photon luminescence emission is strongly mediated by retardation of the excitation field, a consequence of their zero net-dipole moment. This selective excitation of different mode parities is highly relevant for nanoscale enhanced nonlinear optics, as well as plasmonic nanosensor applications and tuning of radiative properties of quantum emitters.

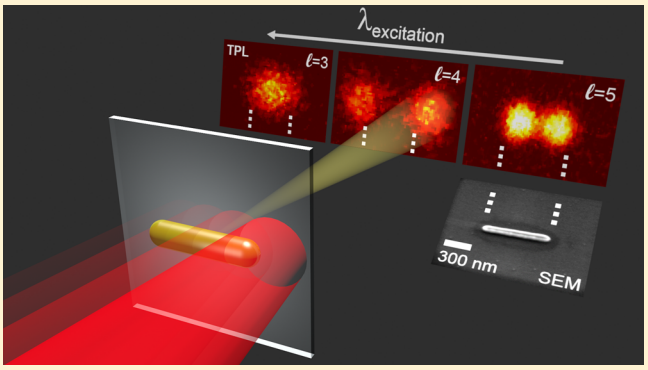

KEYWORDS: *nanoantenna, surface plasmon resonance, higher order modes, two photon luminescence, plasmonics, nonlinear, mode parity*

Metallic nanorods constitute a widely used model system and building blocks for complex optical antenna arrangements.[1−3] As a channel to couple free space radiation to intense, localized optical fields, they offer a broad range of functionalities that are exploited for, for example, directional emission and scattering,[1,4] enhanced Raman scattering,[5] refractive index sensing,[6] coherent ultrafast nanophotonics,[7] tailored spatio and temporal light confinement,[8] slow light metamaterials through electromagnetically induced transparency,[9,10] optical nanocircuits,[11] active photodetection,[12] and nonlinear optics and wave mixing.[13,14]

Typically, only the strong fundamental dipole resonance of the nanorods is considered in antenna designs. Studies on the nonlinear optical properties of plasmonic antennas are mostly limited to the lowest order hybridized mode (bonding mode) in coupled dipole or bowtie antennas owing to the stronger near-field enhancements in the antenna gap region.[15−17] Nevertheless, operating nanorod antennas at higher order modes offers interesting new possibilities such as the generation of multipolar radiation from single quantum emitters,[18,19] or directional emission and scattering by a single-element antenna.[20,21] Moreover, mode parity-controlled Fano- and Lorentz-like resonance line shapes, which offer exciting perspectives for slow-light metamaterials and high sensitivity bio- and chemical-sensing, were recently demonstrated in nanorods.[22−24]

Here, we report on two-photon luminescence (TPL) mediated by higher order antenna modes in gold nanorods. In contrast to second harmonic generation (SHG),[25] local two-photon absorption in gold results in a broadband photoluminescence emission. This TPL is characterized by a quadratic dependence of the emission intensity on the excitation power.[26] It is, consequently, extremely sensitive to the strongly enhanced electromagnetic fields associated with plasmonic excitations in metal nanostructures.[27] These collective oscillations of the free electrons in the metal generate strong TPL signal enhancements in gold nanoparticles such as nanorods, with applications in biological (in vivo) imaging.[28,29] TPL imaging, by scanning a focused laser beam over the sample, has been used to visualize the near-field distributions of localized surface plasmons in, for example, coupled nanorod

Received: December 4, 2014
Published: February 23, 2015

DOI: 10.1021/ph500453m
ACS Photonics 2015, 2, 410−416

antennas,[30−32] bowtie nanoantennas,[27] star-shaped nanoparticle clusters,[33] nanoprisms,[34] and nanovoids.[35] Additionally, TPL microscopy was used to experimentally demonstrate that optical near-field distributions of nanoantennas can be reconfigured with phase-shaped beams.[36] Not only gold, but also aluminum nanorods were found to have a high luminescence efficiency.[37]

In this paper, using scanning laser microscopy, we obtain TPL intensity maps of gold nanorod antennas of varying length. First of all, taking the integrated TPL intensity of each rod allows us to construct an antenna mode dispersion relation from which the contribution of higher order surface plasmon modes to the TPL process is evidenced. Second, the light-antenna coupling is strongly affected by the localized excitation of the focused laser beam, as this allows for phase-retardation of the incident field along the antenna, that is, the optical excitation field is nonuniform on the spatial scale of the nanorod dimensions.[38,39] This is especially important for even parity modes that do not couple to a symmetric excitation such as a normal incident plane wave due to their zero net dipole moment. A mode parity-controlled TPL signal signature related to the light-antenna coupling selection rules is deduced.

In the TPL process, a first near-IR photon excites an intraband transition within the *sp* conduction band, while the second photon drives an interband transition between the *d* and the *sp* bands.[44,45] Following the absorption through interband transitions, the generated electron−hole pairs recombine and emit a photon. The electron-hole recombination occurs near the electronic band structure's *X* and *L* symmetry points giving a broadband emission. For gold, emission peaks are expected at 630 and 520 nm.[44,46,47] A schematic illustration of the plasmonic antenna-mediated two-photon luminescence process and experimental configuration is shown in Figure 1a. A focused laser beam is scanned over the nanorod antenna and the luminescent light is recorded in reflection. A Zeiss LSM 510 Meta scanning laser confocal microscope is used for the experiments. The light of a Spectra Physics Mai Tai DeepSee laser is focus by an Alpha Plan-Apochromat 100× magnification NA = 1.46 oil immersion objective. The laser spot was determined to have a $1/e^2$ diameter of 850 nm at the sample. The reflected light passes a 650 nm edge filter ensuring that only luminescence with wavelengths below 650 nm is detected by the internal detector of the microscope. The nanorods are fabricated using sputter deposition of gold, electron beam lithography, and ion-milling.[40] The rods are 50 nm in height, 70 nm wide, and supported by a thin glass substrate. The sample is organized in arrays consisting of rods with lengths increasing in steps of 20, 30, or 50 nm.

Figure 1b shows the luminescence map for two identical nanorods of length L = 670 nm, rotated by 90° relative to each other, and excited by horizontally polarized light. The orientation of the rods is indicated by their respective SEM image. For the vertical rod, the incident field couples off-resonance to the transverse antenna mode, while for the horizontal rod longitudinal modes are resonantly excited. A clear intensity difference is observed, giving a first indication of the TPL process' dependence on plasmonic resonances.[41] For the horizontal rod, the incident light excites charge density waves at the surface of the metal that form standing wave-like Fabry-Pérot resonances, known as surface plasmon resonances (SPRs).[38] The resonance mode index l is defined as the number of half plasmon wavelengths $\lambda_p/2$ that fit the antenna cavity at

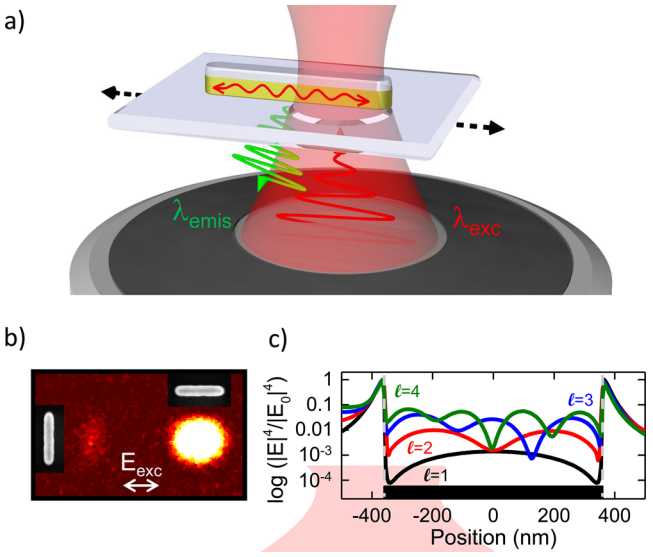

Figure 1. (a) Illustration of the experimental configuration for the investigation of plasmon mediated two-photon luminescence from a gold nanorod antenna. (b) The TPL signal depends on the relative orientation of the nanorod and the light polarization, as shown here for an L = 670 nm rod. The inset SEM images indicate the orientation of the nanorod. (c) Normalized square of the simulated electric field intensity enhancement through the center of the antenna cross-section for the four lowest order antenna modes (log scale). The black box indicates the L = 720 nm antenna edges. The Gaussian excitation beam is focused on the left edge of the antenna.

resonance. At positions where charge accumulates, strong enhancement of the electric near-field occurs outside the antenna, while field minima arise inside. This is illustrated in Figure 1c for the four lowest order SPR antenna modes. Here, the simulated $|E|^4$ profiles taken through the middle of the rod are shown. The mode index is identified from the presented near-field profiles. Simulations in this paper were performed with a commercial FDTD solver[42] using perfectly matched layer (PML) boundaries and a mesh of 5 nm × 5 nm × 2.5 nm covering the nanoantenna. As excitation, a source with Gaussian intensity profile with half width $1/e^2$ of 850 nm was used. In Figure 1c, the source is positioned at the edge of the antenna, as indicated. The permittivity of Au was taken from ref 43, and the refractive index of the substrate was set to n = 1.524.

A TPL scan of three arrays of nanorod antennas taken at λ = 800 nm with horizontal polarization, i.e. along the longitudinal nanorod axis, is shown in Figure 2. The length of the rods is indicated and increases from L = 50 to 1220 nm. Since the TPL emission quadratically depends on the excitation power, resonant structures with strong local fields are clearly distinguished from off-resonant structures that exhibit much lower near-field intensities. Starting from the shortest nanorods (top left) the TPL signal intensity gradually increases until a maximum is reached (black dashed box) and the intensity decreases again. The nanorod at this maximum is resonantly excited by the incident laser light. The very bright rod, marked by the cross, is excluded from further analysis, because the rod's TPL intensity is much brighter for all wavelengths and, as the scanning electron microscopy (SEM) image shows, this particle was damaged, most probably due to laser ablation. For comparison, the antennas shown in the SEM images in Figure 1b and Figure 4 are undamaged. Upon further increase of the

DOI: 10.1021/ph500453m
ACS Photonics 2015, 2, 410−416

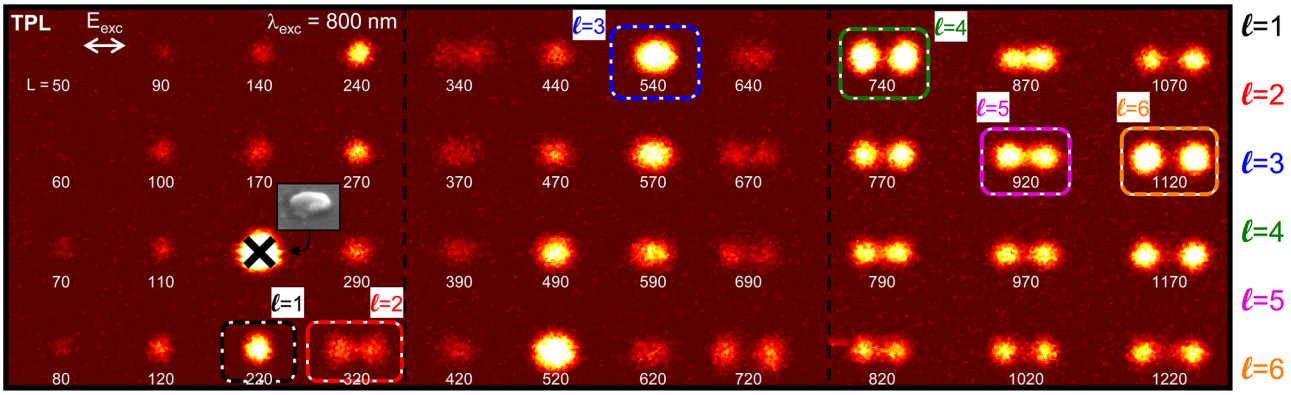

Figure 2. Experimental TPL images where the brightest rods, indicated by the colored dashed boxes, are in resonance. The images are taken at λ = 800 nm excitation wavelength with polarization along the rods axes (horizontal), as indicated. The rods increase in length L from 50 to 1220 nm, as indicated, and are arranged in three arrays (separated by the vertical black dashed lines) that were scanned at different laser powers: 0.185, 0.208, and 0.255 mW from left to right, respectively. The particle marked with the cross is damaged.

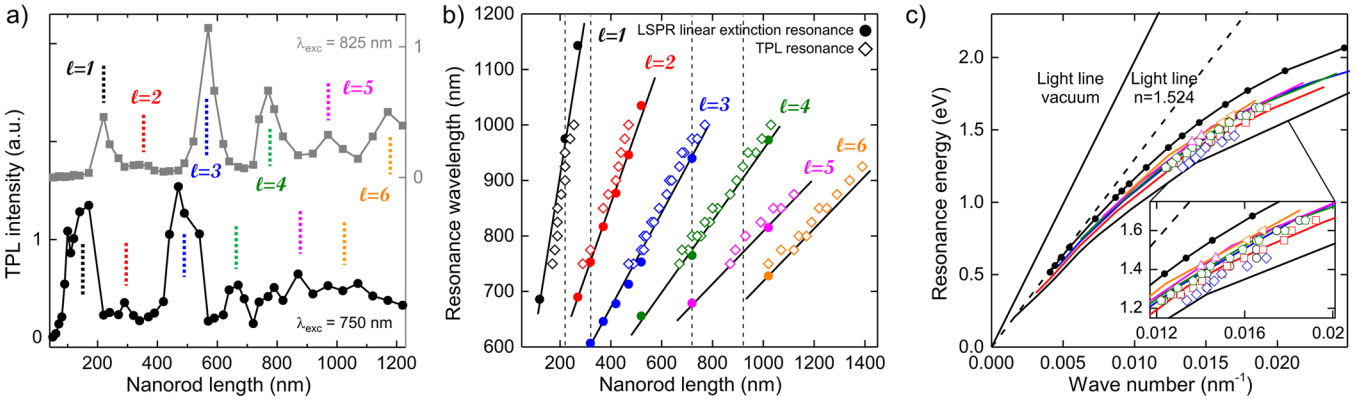

Figure 3. (a) Integrated experimental TPL intensity vs antenna length L for excitation at λ = 750 nm (black dots) and λ = 825 nm (gray squares) reveals the resonant antennas (dashed lines) at the different plasmon modes. (b) The resonance wavelength vs L plot shows the expected linear behavior. Good agreement is observed between linear extinction (full circles) and nonlinear TPL resonances (open diamonds). Full black lines: linear fits to the extinction data. Vertical dashed lines indicate the rod lengths depicted in Figure 4. (c) Dispersion curves showing resonant energy vs mode wavenumber k, defined as $k = \pi l/L$, bend away from the light line, indicating a surface plasmon mediated process. Open symbols: TPL, colored lines: extinction. Straight solid and dashed lines show the light line in vacuum and in n = 1.524 medium, respectively. Black dots: calculated plasmon dispersion of an infinite wire with same cross-sectional geometry as the nanorod antennas.

rod length, two intensity maxima appear (red dashed box) corresponding to the next resonant antenna length. Several additional such maxima can be observed in the scans, as indicated by the dashed boxes, revealing the presence of higher order modes. The specific spatial distribution of the TPL signal will be discussed later. For the moment, the integrated TPL intensity is sufficient to extract resonant antenna lengths and construct a dispersion relation.

To obtain the dispersion relation, the scans in Figure 2 were repeated, and the resonant rods identified, for different excitation wavelengths between λ = 750 and 1000 nm. Figure 3a shows the spatially integrated TPL intensity (over an area similar to the dashed boxes in Figure 2) for each antenna length at excitation wavelengths λ = 750 nm (black dots) and λ = 825 nm (gray squares). The different resonant antenna lengths L appear as peaks in the TPL intensity and are indicated by the dashed lines with the color code as in Figure 2. Plotting the excitation wavelength versus the extracted resonant rod lengths for different wavelengths results in the open diamond data points in Figure 3b. Experimental SPR spectra obtained by linear extinction spectroscopy using a Fourier transform transmission microscope (Bruker vertex 80v + Hyperion)[48] reveal the nanorod SPR mode resonances, as shown by full circles. The expected linear dependence of these modes is clearly observed.[49−51] Moreover, a strong correlation of the TPL resonances with the SPR modes is evident. The TPL resonances nicely follow the linear dispersion of the different nanorod SPR modes, evidencing a plasmon-enhanced two-photon absorption cross-section at the TPL excitation wavelength.[28] Although enhanced photoluminescence emission induced by higher order SPR modes overlapping with the TPL emission bands can not completely be excluded from contributing to the intensity profiles in Figure 3a,[52] its contribution is concluded to be much weaker. Indeed, since each SPR mode order has its characteristic slope in the curves in Figure 3b, a TPL enhancement dominated by higher order SPR modes at the emission band would result in a clear mismatch of the linear (full circles) and TPL (open diamonds) resonances. This data now allows us to assign the proper SPR mode index l to the TPL resonances observed in Figure 2, as indicated. The same color convention for the modes is used throughout the paper.

With this information at hand, the dispersion relation of a gold nanorod can be constructed from both the linear and

DOI: 10.1021/ph500453m
ACS Photonics 2015, 2, 410−416

nonlinear measurements, as shown in Figure 3c. The SPR wavenumber $k = 2\pi/\lambda_p$, with λ_p the SPR wavelength, is defined as $k = \pi l/L$, resulting from the geometrical condition of a standing wave in the antenna cavity.[53,54] Here, L is the antenna length and l the mode index that was determined from Figure 3a. Open symbols correspond to the experimental TPL resonance data shown in Figure 3b, while lines represent the experimental linear extinction spectroscopy data. The straight black solid and dashed lines in Figure 3c are the light lines in vacuum and in a glass medium with refractive index $n = 1.524$, respectively. Solid circles represent the calculated mode dispersion of propagating surface plasmon polaritons (SPPs) in an infinite wire with the same cross-sectional geometry as the nanorods. Both the experimental cavity mode dispersion and calculated SPP dispersion bend to the right of the light line at larger wave numbers illustrating the subwavelength nature of surface plasmons. This excellent agreement between the dispersion curves further demonstrates that the experimentally observed TPL contrast is indeed mapping plasmonic modes in the nanorod antennas and so justifies the standing wave description of the antenna modes.[55]

We can now take a closer look at the TPL images in Figure 2 where different nontrivial TPL intensity distributions can be distinguished for the different SPR mode orders. Figure 4 gives

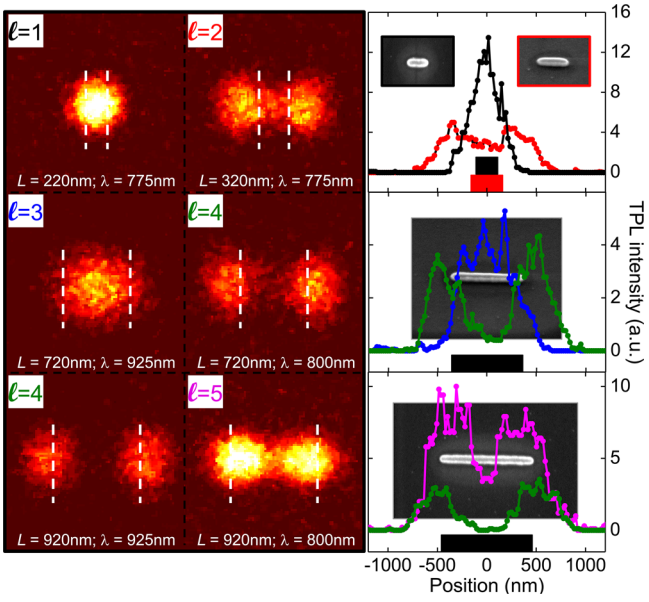

Figure 4. Experimental TPL images for the five lowest order antenna modes (left) with horizontal cross-sectional scans through the center of the bright spots on the right. The nanorod boundaries are indicated with the white dashed lines in the TPL images and the red and black boxes in the graphs. TPL maxima are observed inside the rods for odd modes, while outside for even modes. SEM images of the corresponding antennas are shown in the background.

a more detailed analysis of this observation. Four different antenna lengths at their TPL resonance wavelengths are shown. The associated mode orders are extracted from Figure 3b (dashed lines). On the right of Figure 4, the corresponding TPL intensity line scans through the middle of the antennas are shown, as well as an SEM image. The white dashed lines and black and red boxes indicate the antenna edges. An accurate calibration of the experimental scan dimensions is obtained from the well-defined pitch of the antenna arrays. The most notable observation here is the fact that for odd order modes (l = 1, 3, and 5) the TPL maxima are located within the boundaries of the nanorod, while outside for the even parity modes (l = 2 and 4), marking a clear signature of the mode parity.

To correlate the TPL intensity distribution directly with the near-field distribution of the plasmonic nanostructures, considering the quadratic power dependence, usually the TPL signal is compared with the $|E|^4$ field maps of the plasmonic system. Nonetheless, the diffraction limited spatial resolution requires that comparison should at least be made through a convolution of the field maps with the Gaussian intensity profile of the incident laser beam.[31] For the l = 1 and 3 modes (black and blue curves, respectively), the single central TPL hotspot could be explained by the limited spatial resolution of the experiment. Indeed, convoluting the modes' near-field distributions shown in Figure 1c with the Gaussian excitation profile will result in a single peak. However, for the l = 2 and 4 modes (red and green curves, respectively), two clear maxima exist outside of the antenna. Since near-field decay lengths and enhancement factors do not significantly depend on the antenna mode parity (see Figure 1c), the resulting TPL maps can not properly be described by a mere Gaussian convolution of the $|E|^4$ mode maps shown in Figure 1c.

To obtain a more detailed and accurate description of the light−matter interaction in the TPL process, we simulate the system for each scan location of a Gaussian light beam excitation and integrate the near-field intensity inside the metal (Figure 5).[32,56] As such, the contribution of the phase-

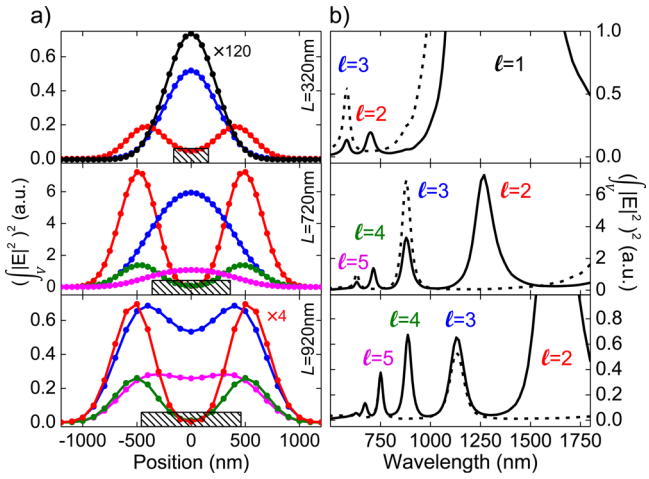

Figure 5. (a) Simulated $(\int_V |E|^2)^2$ intensity profiles corresponding to Figure 4 accurately reproduce the experimental results. Colors indicate the SPR mode order. The box indicates for each panel the nanorod size. (b) $(\int_V |E|^2)^2$ spectra corresponding to (a) for excitation at dashed line: the center of the nanorod (x = 0 nm), and full line: off-center with position x = 400, 450, and 500 nm for L = 320, 720, and 920 nm, respectively.

retardation induced by the localized excitation is taken into account in the light-antenna coupling efficiency. Since we are interested in a surface plasmon mediated two-photon absorption process, for our analysis, we assume that the luminescence originates only from absorbed plasmon excitations in the metal. The absorption of an excited surface plasmon is proportional to $\int_V |E|^2$, where V is the antenna volume. A two-photon absorption process will therefore be proportional to $(\int_V |E|^2)^2$.[32]

DOI: 10.1021/ph500453m
ACS Photonics 2015, 2, 410−416

The simulated $(\int_V |E|^2)^2$ profiles corresponding to Figure 4 are shown in Figure 5a. They accurately reproduce the experimental results. Note that the simulations only take the excitation path of the TPL process into account. The good agreement with the experimental maps therefore indicates that the experimentally observed characteristic TPL features are not determined by the collection path, but by the excitation efficiency.[31]

For the shortest rods in Figures 4 and 5, the two TPL maxima located outside of the rods for the $l = 2$ and 4 modes can now be explained as follows. Their even parity dictates that these modes will not couple to a normal incident plane wave or a symmetric dipolar excitation.[38,39] The result is a low TPL signal excited by the focused laser spot positioned in the center of the rod. Since the $l = 1$ mode has a low quality factor, its tail will have a small spectral overlap with the $l = 2$ mode, preventing the signal from completely dropping to zero for $l = 2$. For the spatially confined field of the laser, the dipole approximation no longer holds and when moving the laser away from the center of the rod, the symmetry of the system is broken. Now coupling to the even order SPR modes is allowed through phase-retardation, giving rise to the observed gradual increase in the TPL signal. The signal intensity increases until an optimum phase-matching and coupling efficiency is reached. Remarkably, this optimum is reached when the laser is positioned outside of the antenna boundary, up to ~200 nm for $L = 320$ nm and ~140 nm for $L = 720$ nm, where the near-field has already strongly decayed.

For the longer antenna of length $L = 920$ nm (bottom graphs in Figures 4 and 5), also the odd $l = 3$ (blue) and 5 (pink) modes show two maxima. This observation could be interpreted as the dominant $|E|^4$ maxima at the rod edges (see Figure 1c) that start to be resolved as the rod length increases. Another way of interpreting this edge effect is by considering the antenna as a long nanowire which is most efficiently excited at its edges.[57] Nevertheless, these odd mode TPL maxima are located within the antenna boundaries, in strong contrast to what is observed for the even modes.

The spectral dependence of $(\int_V |E|^2)^2$ is shown in Figure 5b, revealing the spectral position of the modes in (a). Dashed curves correspond to a symmetric excitation located at $x = 0$ nm, hence, not exciting even parity modes, while the full curves are taken at the position of the TPL maxima at the antenna edges. The symmetry breaking introduced by moving the excitation off-center in the latter case allows coupling to the even modes. The spectra further indicate that the modes have only a weak spectral overlap, allowing their respective TPL maps to be easily distinguishable experimentally.

In conclusion, we have established a clear link between higher order surface plasmon resonances and two-photon absorption in gold nanoantennas by constructing a plasmon dispersion curve based on nonlinear TPL scanning laser microscopy measurements. An excellent match with the antennas' plasmonic modes obtained by linear extinction spectroscopy was found. Additionally, a clear signature of the mode parity was observed in the TPL images. TPL intensity maxima were found to be located within the antenna boundaries for odd modes, while outside for even order modes. The experimental maps could be reproduced by the square of the integrated field intensity enhancement inside the antenna, calculated at every position of the Gaussian excitation beam using FDTD simulations. Convolution with the antenna's near-field distribution does not give a proper description of the TPL process in the case of even parity modes where retardation effects by symmetry breaking of the illumination strongly affects the light-antenna coupling and, hence, SPR excitation efficiency. Our findings suggest that the nature of the surface plasmon modes in metal nanoparticles can play a crucial role in the optimization of plasmon-enhanced nonlinear optics, where even parity modes present interesting possibilities due to their zero net dipole moment and related radiative properties.

AUTHOR INFORMATION

Corresponding Author

*E-mail: niels.verellen@imec.be.

Notes

The authors declare no competing financial interest.

ACKNOWLEDGMENTS

N.V. acknowledges the F.W.O. Flanders for financial support. N.V., D.D., and V.V.M. are supported by the Methusalem funding by the Flemish Government. B.D.C. and M.A. gratefully acknowledge the support by tUL-impulse phase II. The work of A.V.S. was partially supported by "Mandat d'Impulsion Scientifique" of the F.R.S.-FNRS. The authors thank Ventsislav K. Valev for his assistance with the TPL measurements, Jos Moonens for e-beam assistance, and Karen Levrie for graphical support.

REFERENCES

(1) Curto, A. G.; Volpe, G.; Taminiau, T. H.; Kreuzer, M. P.; Quidant, R.; van Hulst, N. F. Unidirectional Emission of a Quantum Dot Coupled to a Nanoantenna. *Science* **2010**, *329*, 930−933.

(2) Valev, V. K.; et al. Nanostripe Length Dependence of Plasmon-Induced Material Deformations. *Opt. Lett.* **2013**, *38*, 2256−2258.

(3) Denkova, D.; Verellen, N.; Silhanek, A. V.; Van Dorpe, P.; Moshchalkov, V. V. Lateral Magnetic Near-Field Imaging of Plasmonic Nanoantennas with Increasing Complexity. *Small* **2014**, *10*, 1959−1966.

(4) Kosako, T.; Kadoya, Y.; Hofmann, H. F. Directional Control of Light by a Nano-Optical Yagi-Uda Antenna. *Nat. Photonics* **2010**, *4*, 312−315.

(5) Toma, A.; Das, G.; Chirumamilla, M.; Saeed, A.; Zaccaria, R. P.; Razzari, L.; Leoncini, M.; Liberale, C.; Angelis, F. D.; Fabrizio, E. D. Fabrication and Characterization of a Nanoantenna-Based Raman Device for Ultrasensitive Spectroscopic Applications. *Microelectron. Eng.* **2012**, *98*, 424−427.

(6) Tian, L.; Chen, E.; Gandra, N.; Abbas, A.; Singamaneni, S. Gold Nanorods as Plasmonic Nanotransducers: Distance-Dependent Refractive Index Sensitivity. *Langmuir* **2012**, *28*, 17435−17442.

(7) Brinks, D.; Castro-Lopez, M.; Hildner, R.; van Hulst, N. F. Plasmonic Antennas as Design Elements for Coherent Ultrafast Nanophotonics. *Proc. Natl. Acad. Sci. U.S.A.* **2013**, *110*, 18386−18390.

(8) Hanke, T.; Cesar, J.; Knittel, V.; Trügler, A.; Hohenester, U.; Leitenstorfer, A.; Bratschitsch, R. Tailoring Spatiotemporal Light Confinement in Single Plasmonic Nanoantennas. *Nano Lett.* **2012**, *12*, 992−996.

(9) Zhang, S.; Genov, D. A.; Wang, Y.; Liu, M.; Zhang, X. Plasmon-Induced Transparency in Metamaterials. *Phys. Rev. Lett.* **2008**, *101*, 047401.

(10) Liu, N.; Langguth, L.; Weiss, T.; Kastel, J.; Fleischhauer, M.; Pfau, T.; Giessen, H. Plasmonic Analogue of Electromagnetically Induced Transparency at the Drude Damping Limit. *Nat. Mater.* **2009**, *8*, 758−762.

(11) Huang, J.-S.; Feichtner, T.; Biagioni, P.; Hecht, B. Impedance Matching and Emission Properties of Nanoantennas in an Optical Nanocircuit. *Nano Lett.* **2009**, *9*, 1897−1902.

DOI: 10.1021/ph500453m
ACS Photonics 2015, 2, 410−416

(12) Knight, M. W.; Sobhani, H.; Nordlander, P.; Halas, N. J. Photodetection with Active Optical Antennas. *Science* **2011**, *332*, 702−704.
(13) Harutyunyan, H.; Volpe, G.; Quidant, R.; Novotny, L. Enhancing the Nonlinear Optical Response Using Multifrequency Gold-Nanowire Antennas. *Phys. Rev. Lett.* **2012**, *108*, 217403.
(14) Maksymov, I. S.; Miroshnichenko, A. E.; Kivshar, Y. S. Cascaded Four-Wave Mixing in Tapered Plasmonic Nanoantenna. *Opt. Lett.* **2013**, *38*, 79−81.
(15) Kim, S.; Jin, J.; Kim, Y.-J.; Park, I.-Y.; Kim, Y.; Kim, S.-W. High-Harmonic Generation by Resonant Plasmon Field Enhancement. *Nature* **2008**, *453*, 757−760.
(16) Abb, M.; Albella, P.; Aizpurua, J.; Muskens, O. L. All-Optical Control of a Single Plasmonic Nanoantenna-ITO Hybrid. *Nano Lett.* **2011**, *11*, 2457−2463.
(17) Ko, K. D.; Kumar, A.; Fung, K. H.; Ambekar, R.; Liu, G. L.; Fang, N. X.; Toussaint, K. C. Nonlinear Optical Response from Arrays of Au Bowtie Nanoantennas. *Nano Lett.* **2011**, *11*, 61−65.
(18) Taminiau, T. H.; Stefani, F. D.; van Hulst, N. F. Optical Nanorod Antennas Modeled as Cavities for Dipolar Emitters: Evolution of Sub- and Super-Radiant Modes. *Nano Lett.* **2011**, *11*, 1020−1024.
(19) Curto, A. G.; Taminiau, T. H.; Volpe, G.; Kreuzer, M. P.; Quidant, R.; van Hulst, N. F. Multipolar Radiation of Quantum Emitters with Nanowire Optical Antennas. *Nat. Commun.* **2013**, *4*, 1750.
(20) Vercruysse, D.; Sonnefraud, Y.; Verellen, N.; Fuchs, F. B.; Di Martino, G.; Lagae, L.; Moshchalkov, V. V.; Maier, S. A.; Van Dorpe, P. Unidirectional Side Scattering of Light by a Single-Element Nanoantenna. *Nano Lett.* **2013**, *13*, 3843−3849.
(21) Vercruysse, D.; Zheng, X.; Sonnefraud, Y.; Verellen, N.; Di Martino, G.; Lagae, L.; Vandenbosch, G. A. E.; Moshchalkov, V. V.; Maier, S. A.; Van Dorpe, P. Directional Fluorescence Emission by Individual V-Antennas Explained by Mode Expansion. *ACS Nano* **2014**, *8*, 8232−8241.
(22) López-Tejeira, F.; Paniagua-Domínguez, R.; Rodríguez-Oliveros, R.; Sánchez-Gil, J. A. Fano-Like Interference of Plasmon Resonances at a Single Rod-Shaped Nanoantenna. *New J. Phys.* **2012**, *14*, 023035.
(23) López-Tejeira, F.; Paniagua-Domínguez, R.; Sánchez-Gil, J. A. High-Performance Nanosensors Based on Plasmonic Fano-Like Interference: Probing Refractive Index with Individual Nanorice and Nanobelts. *ACS Nano* **2012**, *6*, 8989−8996.
(24) Verellen, N.; López-Tejeira, F.; Paniagua-Domínguez, R.; Vercruysse, D.; Denkova, D.; Lagae, L.; Van Dorpe, P.; Moshchalkov, V. V.; Sánchez-Gil, J. A. Mode Parity-Controlled Fano- and Lorentz-Like Line Shapes Arising in Plasmonic Nanorods. *Nano Lett.* **2014**, *14*, 2322−2329.
(25) Valev, V. K. Characterization of Nanostructured Plasmonic Surfaces with Second Harmonic Generation. *Langmuir* **2012**, *28*, 15454−15471.
(26) Beversluis, M. R.; Bouhelier, A.; Novotny, L. Continuum Generation from Single Gold Nanostructures through Near-Field Mediated Intraband Transitions. *Phys. Rev. B* **2003**, *68*, 115433.
(27) Schuck, P. J.; Fromm, D. P.; Sundaramurthy, A.; Kino, G. S.; Moerner, W. E. Improving the Mismatch between Light and Nanoscale Objects with Gold Bowtie Nanoantennas. *Phys. Rev. Lett.* **2005**, *94*, 017402.
(28) Wang, H.; Huff, T. B.; Zweifel, D. A.; He, W.; Low, P. S.; Wei, A.; Cheng, J.-X. In Vitro and In Vivo Two-Photon Luminescence Imaging of Single Gold Nanorods. *Proc. Natl. Acad. Sci. U.S.A.* **2005**, *102*, 15752−15756.
(29) Wang, T.; Halaney, D.; Ho, D.; Feldman, M. D.; Milner, T. E. Two-Photon Luminescence Properties of Gold Nanorods. *Biomed. Opt. Express* **2013**, *4*, 584−595.
(30) Mühlschlegel, P.; Eisler, H.-J.; Martin, O. J. F.; Hecht, B.; Pohl, D. W. Resonant Optical Antennas. *Science* **2005**, *308*, 1607−1609.
(31) Ghenuche, P.; Cherukulappurath, S.; Taminiau, T. H.; van Hulst, N. F.; Quidant, R. Spectroscopic Mode Mapping of Resonant Plasmon Nanoantennas. *Phys. Rev. Lett.* **2008**, *101*, 116805.
(32) Huang, J.-S.; Kern, J.; Geisler, P.; Weinmann, P.; Kamp, M.; Forchel, A.; Biagioni, P.; Hecht, B. Mode Imaging and Selection in Strongly Coupled Nanoantennas. *Nano Lett.* **2010**, *10*, 2105−2110.
(33) Ghenuche, P.; Cherukulappurath, S.; Quidant, R. Mode Mapping of Plasmonic Stars Using TPL Microscopy. *New J. Phys.* **2008**, *10*, 105013.
(34) Viarbitskaya, S.; Teulle, A.; Marty, R.; Sharma, J.; Girard, C.; Arbouet, A.; Dujardin, E. Tailoring and Imaging the Plasmonic Local Density of States in Crystalline Nanoprisms. *Nat. Mater.* **2013**, *12*, 426−432.
(35) Imura, K.; Ueno, K.; Misawa, H.; Okamoto, H. Optical Field Imaging of Elongated Rectangular Nanovoids in Gold Thin Film. *J. Phys. Chem. C* **2013**, *117*, 2449−2454.
(36) Volpe, G.; Cherukulappurath, S.; Juanola Parramon, R.; Molina-Terriza, G.; Quidant, R. Controlling the Optical Near Field of Nanoantennas with Spatial Phase-Shaped Beams. *Nano Lett.* **2009**, *9*, 3608−3611.
(37) Castro-Lopez, M.; Brinks, D.; Sapienza, R.; van Hulst, N. F. Aluminum for Nonlinear Plasmonics: Resonance-Driven Polarized Luminescence of Al, Ag, and Au Nanoantennas. *Nano Lett.* **2011**, *11*, 4674−4678.
(38) Dorfmüller, J.; Vogelgesang, R.; Khunsin, W.; Rockstuhl, C.; Etrich, C.; Kern, K. Plasmonic Nanowire Antennas: Experiment, Simulation, and Theory. *Nano Lett.* **2010**, *10*, 3596−3603.
(39) Denkova, D.; Verellen, N.; Silhanek, A. V.; Valev, V. K.; Van Dorpe, P.; Moshchalkov, V. V. Mapping Magnetic Near-Field Distributions of Plasmonic Nanoantennas. *ACS Nano* **2013**, *7*, 3168−3176.
(40) Verellen, N.; Sonnefraud, Y.; Sobhani, H.; Hao, F.; Moshchalkov, V. V.; Van Dorpe, P.; Nordlander, P.; Maier, S. A. Fano Resonances in Individual Coherent Plasmonic Nanocavities. *Nano Lett.* **2009**, *9*, 1663−1667.
(41) Bouhelier, A.; Bachelot, R.; Lerondel, G.; Kostcheev, S.; Royer, P.; Wiederrecht, G. P. Surface Plasmon Characteristics of Tunable Photoluminescence in Single Gold Nanorods. *Phys. Rev. Lett.* **2005**, *95*, 267405.
(42) Lumerical Solutions; http://www.lumerical.com (accessed December 3, 2014).
(43) Johnson, P. B.; Christy, R. W. Optical Constants of the Noble Metals. *Phys. Rev. B* **1972**, *6*, 4370−4379.
(44) Imura, K.; Nagahara, T.; Okamoto, H. Near-Field Two-Photon-Induced Photoluminescence from Single Gold Nanorods and Imaging of Plasmon Modes. *J. Phys. Chem. B* **2005**, *109*, 13214−13220.
(45) Biagioni, P.; Celebrano, M.; Savoini, M.; Grancini, G.; Brida, D.; Mátéfi-Tempfli, S.; Mátéfi-Tempfli, M.; Duò, L.; Hecht, B.; Cerullo, G.; Finazzi, M. Dependence of the Two-Photon Photoluminescence Yield of Gold Nanostructures on the Laser Pulse Duration. *Phys. Rev. B* **2009**, *80*, 045411.
(46) Roaf, D. J. The Fermi Surfaces of Copper, Silver and Gold II. Calculation of the Fermi Surfaces. *Philos. Trans. R. Soc. London* **1962**, *255*, 135−152.
(47) Knittel, V.; Fischer, M. P.; de Roo, T.; Mecking, S.; Leitenstorfer, A.; Brida, D. Nonlinear Photoluminescence Spectrum of Single Gold Nanostructures. *ACS Nano* **2015**, *9*, 894−900.
(48) Verellen, N.; Van Dorpe, P.; Vercruysse, D.; Vandenbosch, G. A. E.; Moshchalkov, V. V. Dark and Bright Localized Surface Plasmons in Nanocrosses. *Opt. Express* **2011**, *19*, 11034−11051.
(49) Novotny, L. Effective Wavelength Scaling for Optical Antennas. *Phys. Rev. Lett.* **2007**, *98*, 266802.
(50) Neubrech, F.; Weber, D.; Lovrincic, R.; Pucci, A.; Lopes, M.; Toury, T.; de La Chapelle, M. L. Resonances of Individual Lithographic Gold Nanowires in the Infrared. *Appl. Phys. Lett.* **2008**, *93*, 163105.
(51) Olmon, R. L.; Krenz, P. M.; Jones, A. C.; Boreman, G. D.; Raschke, M. B. Near-Field Imaging of Optical Antenna Modes in the Mid-Infrared. *Opt. Express* **2008**, *16*, 20295−20305.
(52) Imura, K.; Okamoto, H. Properties of Photoluminescence from Single Gold Nanorods Induced by Near-Field Two-Photon Excitation. *J. Chem. Phys. C* **2009**, *113*, 11756−11759.

DOI: 10.1021/ph500453m
ACS Photonics 2015, 2, 410−416

(53) Imura, K.; Nagahara, T.; Okamoto, H. Near-Field Optical Imaging of Plasmon Modes in Gold Nanorods. *J. Chem. Phys.* **2005**, *122*, 154701.
(54) Vesseur, E. J. R.; de Waele, R.; Kuttge, M.; Polman, A. Direct Observation of Plasmonic Modes in Au Nanowires Using High-Resolution Cathodoluminescence Spectroscopy. *Nano Lett.* **2007**, *7*, 2843−2846.
(55) Schider, G.; Krenn, J. R.; Hohenau, A.; Ditlbacher, H.; Leitner, A.; Aussenegg, F. R.; Schaich, W. L.; Puscasu, I.; Monacelli, B.; Boreman, G. Plasmon Dispersion Relation of Au and Ag Nanowires. *Phys. Rev. B* **2003**, *68*, 155427.
(56) Teulle, A.; Marty, R.; Viarbitskaya, S.; Arbouet, A.; Dujardin, E.; Girard, C.; des Francs, G. C. Scanning Optical Microscopy Modeling in Nanoplasmonics. *J. Opt. Soc. Am. B* **2012**, *29*, 2431−2437.
(57) Ditlbacher, H.; Hohenau, A.; Wagner, D.; Kreibig, U.; Rogers, M.; Hofer, F.; Aussenegg, F. R.; Krenn, J. R. Silver Nanowires as Surface Plasmon Resonators. *Phys. Rev. Lett.* **2005**, *95*, 257403.

DOI: 10.1021/ph500453m
ACS Photonics 2015, 2, 410−416